Implications for the origin and evolution of Martian recurring slope lineae at Hale crater from CaSSIS observations

G. Munaretto[a,b,*], M. Pajola[a], G. Cremonese[a], C. Re[a], A. Lucchetti[a], E. Simioni[a], A. S. McEwen[c], A. Pommerol[d], P. Becerra[d], S. J. Conway[e], N. Thomas[d], M. Massironi[a,f]

[a]*INAF, Osservatorio Astronomico di Padova, Padova, Italy*
[b]*Department of Physics and Astronomy "G. Galilei", University of Padova, Padova, Italy*
[c]*Lunar and Planetary Laboratory, University of Arizona, Tucson, Arizona, USA*
[d]*Physikalisches Institut Universität Bern, Switzerland*
[e]*CNRS Laboratoire de Planétologie et Géodynamique de Nantes, Université de Nantes, 2 rue de la Houssiniére, 44322 Nantes, France*
[f]*Department of Geosciences, University of Padova, Padova, Italy*

Abstract

Recurring Slope Lineae (RSL) are narrow, dark features that typically source from rocky outcrops, incrementally lengthen down Martian steep slopes in warm seasons, fade in cold seasons and recur annually. In this study we report the first observations of RSL at Hale crater, Mars, during late southern summer by the Colour and Surface Science Imaging System (CaSSIS) on board ESA's ExoMars Trace Gas Orbiter (TGO). For the first time, we analyze images of RSL acquired during morning solar local times and compare them with High Resolution Imaging Science Experiment (HiRISE) observations taken in the afternoon. We find that RSL activity is correlated with the presence of steep slopes. Our thermal analysis establishes that local temperatures are high enough to allow either the melting of brines or deliquescence

*Corresponding author
Email address: giovanni.munaretto.1@phd.unipd.it, munarettogiovanni@gmail.com (G. Munaretto)

of salts during the observation period, but the slope and aspect distributions of RSL activity predicted by these processes are not consistent with our observations. We do not find any significant relative albedo difference between morning and afternoon RSL. Differences above 11% would have been detected by our methodology, if present. This instead suggests that RSL at Hale crater are not caused by seeping water that reaches the surface, but are best explained as dry flows of granular material.
Keywords: Recurring slope Lineae, RSL, CaSSIS, HiRISE, Mars, Relative albedo, THEMIS

1. Introduction

The origin of Recurring Slope Lineae (RSL) is one of the most controversial science questions regarding present-day surface activity on Mars. They appear as narrow (< 5 m) low-albedo streaks, often starting from bedrock outcrops and lengthening hundreds of meters down Martian steep slopes at equatorial and mid-latitudes (McEwen et al., 2011). RSL generally start lengthening during warm seasons, fade during cold ones and and recur over multiple Martian years. However, RSL activity can be more complicated than a simple repeating cycle of lengthening and fading, as several well studied sites shows simultaneous lengthening, appearance and fading of RSL (Stillman and Grimm, 2018; Vincendon et al., 2019). Many models have been proposed to explain their origin, but a definitive explanation is still elusive. These can be broadly summarized in three classes: *wet models*, in which RSL are water-dominated features, *dry models*, that explain RSL as dry mass fluxes or aeolian features, and *hybrid models*, in which water plays an indirect role in RSL formation and lengthening.

1.1. *Wet models*

The temperature dependence of RSL activity suggests that water or brines may be present (McEwen et al., 2011; McEwen et al., 2014; Stillman et al., 2014; Huber et al., 2020). Spatial correlation with multi-scale fractures appears to support groundwater sources (Stillman et al., 2016; Abotalib and Heggy, 2019). However, topographic relationships cast doubts on these models, as they explain the seasonality of RSL activity, but require larger volumes of liquids than could be reasonably present on Mars at these latitudes (Grimm et al., 2014; Chojnacki et al., 2016). Moreover, many RSL source from local topographic highs, such as ridge crests or peaks, where a groundwater source is unlikely (Chojnacki et al., 2016). Another wet process that has been considered to explain RSL formation is the deliquescence of salts, which occurs when hygroscopic salts absorb water vapor to form a liquid solution (Gough et al., 2016). For this to happen, temperatures higher than the eutectic temperature of the solution and relative humidities (RH) greater than their deliquescence relative humidity (DRH) are required (Gough et al., 2016). Several laboratory studies have identified chlorides (Gough et al., 2016; Wang et al., 2019), perchlorates (Nuding et al., 2014) and chlorates (Toner and Catling, 2018) as potential candidate deliquescent salts. The required RH values for the deliquescence of $CaCl_2$ brines range from 12.9% when $T = 273$ K to $\sim 20.9\%$ at $T = 233$ K (Gough et al., 2016), while their eutectic temperature is $T = 223K$. Numerical modeling by Gough et al. (2016) showed that atmospheric water vapor could sustain the deliquescence of hydrated $CaCl_2$ brines at 3-cm depth at the Phoenix landing site. However, it is not clear whether or not the same process can happen at RSL sites (Gough et al., 2016), even though Wang et al. (2019) recently proposed that the deliquescence of subsurface hydrated chlorides can be a thermodynamically viable (but not necessarily sufficient) process for triggering RSL activity. The deliquescence of Ca-perchlorates is also interesting because of their realtively low DRH (from $10 \pm 4\%$ at 273 K to $55 \pm 4\%$ at 223 K (Nuding et al., 2014)) and eutectic temperature of $T = 200$ K. Finally, chlorates may be even more interesting candidates as they have a lower DRH than perchlorates (Toner and Catling, 2018).

1.2. Dry models

In these models, RSL lengthening and formation are interpreted with dry mechanisms involving granular flows or aeolian processes (Dundas et al., 2017; Schmidt et al., 2017; Vincendon et al., 2019; Schaefer et al., 2019). These have been initially invoked to explain the correlation between the angle of repose of granular material and the slope angle at which RSL stop (Dundas et al., 2017), although more recent measurements show that $\sim 25\%$ of RSL reach slopes below the angle of repose (Tebolt et al., 2020; Stillman et al., 2020). In addition, Schmidt et al. (2017) discussed morphological inconsistencies between RSL and wet flows, such as the lack of terminal or lateral levees; Vincendon et al. (2019) proved that RSL formation occurs outside the time-frame compatible with the existence of liquid water and does not show a preference for the warmest slopes. Finally, the spectral detection of hydrated salts at some RSL sites (Ojha et al., 2015), which would support the presence of liquids, was recently proven to not be robust (Leask et al., 2018; Vincendon et al., 2019). Although dry flows do not require a source of water, a trigger mechanism has not been fully established yet. Schmidt et al. (2017) proposed a Knudsen pump as a trigger mechanism, but it doesn't predict RSL at the times and locations where they are observed (Stillman and Grimm, 2018; Vincendon et al., 2019). Vincendon et al. (2019) and Schaefer et al. (2019) proposed that RSL are aeolian features resulting from the removal of bright dust by winds. A fading mechanism has been recently proposed by Vincendon et al. (2019), which showed that the progressive brightening of RSL can be attributed to dust deposition. On the other hand Schaefer et al. (2019) discovered that the fading of RSL is similar to that of other dust-related albedo features (dust devil tracks, rockfalls) on the basis of relative albedo analyses at Tivat crater (45° S, 9° E). They propose that RSL fade due to the widespread removal of dust from the neighboring slopes, which progressively darken until matching the RSL reflectance. While this mechanism applies well to Tivat crater, it cannot explain the concurrent fading and lengthening of RSL observed in several other RSL sites (Vincendon et al., 2019; Stillman et al., 2020).

1.3. Hybrid models

Other hypotheses envision an indirect role of water in triggering RSL activity. Massé et al. (2016) showed that boiling fresh water can trigger granular flows by violently displacing grains. While this model is interesting because it requires less water than wet-based models, boiling water requires high temperatures that are hardly met at the onset of RSL activity in early spring (Stillman and Grimm, 2018; Vincendon et al., 2019). More recently, Shoji et al. (2019) proposed that moisture serves to stabilize steep slopes in cold seasons, which flow when drying during the warm seasons. In addition, Bishop et al. (2019) proposed that subsurface brine activity can create surface collapse features, perhaps initiating RSL when on steep enough slopes.

The High Resolution Imaging Science Experiment (HiRISE, McEwen et al. (2007)) on board the NASA's Mars Reconnaissance Orbiter (MRO) mission is the optimal instrument to image RSL due to its high pixel scale ($\sim$ 0.3 m/pixel), which allows for digital terrain models (DTM) at $\sim$ 1 m spatial resolution. However, the Sun-synchronous orbit of MRO limits observation times between $\sim$ 2-4 PM, during the local afternoon.

The Colour and Surface Imaging System (CaSSIS, Thomas et al. (2017)), on board the ESA ExoMars Trace Gas Orbiter (TGO) mission, images the Martian surface at 4.6 m/pixel in four color bands. It carries a rotation mechanism that allows it to acquire stereo observations with identical illumination angles for the production of DTMs. The 74° inclined orbit of TGO allows CaSSIS to observe the surface at different times of day, such as the local morning. This capability is pivotal for RSL studies, since morning observations of these features are not possible otherwise. The only exceptions are extremely early morning views by Mars Odyssey, with poor SNR and much lower spatial resolution. Morning activity can provide great insights on the nature and formation mechanism of RSL. Laboratory studies (Gough et al., 2016) and analyses of data from both the Rover Environmental Monitoring Station (REMS) on board Curiosity and the Thermal and Electrical Conductivity Probe (TECP) on the Phoenix lander shows that daily maximum RH values occur during the early morning of local summer (Steele et al., 2017; Fischer et al., 2019), suggesting that these local hours are the most favourable for deliquescence. If RSL are liquid-based flows, their activity should increase in the morning, when both temperature and air humidity are high enough to favor the deliquescence of salts and increase the stability of brines. Under this scenario, dehydration would occur in the afternoon, so we would also expect RSL to be darker in the morning than in the afternoon. Instead, if RSL are caused by the melting of shallow subsurface ice (such as from a deep groundwater source), then they should be darker in the afternoon. This assumes that the quantity of water or brines at play is relatively small, so that evaporative losses exceed the supply of water (Hillel, 2004). If instead RSL have a high water content, pore water concentration would not be affected by evaporation and there wouldn't be any albedo change (Pommerol et al., 2013; Levy et al., 2014). The latter case, however, may not be in agreement with the very low water content of RSL estimated at Garni crater (Edwards and Piqueux, 2016). Finally, if RSL are dry flows, then we do not expect any albedo change between the observations.

In this study we present the first observations of RSL performed by CaSSIS during the local morning and compare them with HiRISE observations acquired one month earlier in the afternoon. In particular, we search for any differences in their overall morphology (i.e. length, slope, aspect) and report relative albedo measurements performed on morning and afternoon images. We analyze the thermal conditions of the surface and shallow sub-surface at the time of the CaSSIS observation to assess whether temperatures would either allow melting of brines or deliquescence of salts.

2. Data

The study region is the central peak of Hale crater ($-35.7°$ N, $323.5°$ E, see figures (2a, b)), where several areally extensive RSL have been discovered so far, making it an ideal site to be investigated with CaSSIS. RSL in Hale were first reported by Ojha et al. (2014) and then analyzed by different authors (Stillman et al., 2014; Dundas et al., 2017; Stillman and Grimm, 2018). Stillman and Grimm (2018) reported that RSL activity in general may occur in one or two pulses, where RSL fade partially or completely and then re-appear in the same year. The RSL at Hale crater are peculiar because they seem to experience three pulses of activity (Stillman and Grimm, 2018), unlike any other sites analyzed on Mars so far. Our RSL observations span an L_s range between 331.5° and 347.4°, within the third pulse proposed by Stillman and Grimm (2018), allowing us to confirm its presence at Hale crater. In order to study whether there is a diurnal dependence in the activity of RSL, an ideal dataset would include two observations of an RSL site acquired during the same Martian day, the first one with CaSSIS in the morning and the second one with HiRISE in the afternoon. In our case, the observations were acquired during late southern summer, one month apart. The HiRISE image was acquired on $L_s = 331.5°$ at 14:06 local time, while the CaSSIS image was acquired on $L_s = 347.4°$ at 11:13 local time. This time interval may be too big to minimize seasonal changes between images, such as fading of RSL, which typically happens during this season at southern hemisphere sites. However, this issue may not be important for Hale crater, where fading was reported to occur only after $L_s > 7°$ for both MY 30 and 31 (Stillman and Grimm, 2018), well after the L_s of our observations. For this reason, we are confident that fading is not influencing our analysis. Moreover, RSL at Hale crater are "rejuvenated" by a third pulse of activity which occurs just before $L_s = 331.5°$. The occurrence of this third pulse of activity is illustrated in figure (1). HiRISE image ESP_057_569_1440, acquired at $L_s = 286.6°$, shows dense RSL coverage (see fig. 1a), while the subsequent HiRISE image ESP_058618_1445, acquired at $L_s = 331.5°$, shows smaller RSL in the same places (see fig. 1b). These further lengthened in the subsequent CaSSIS image MY34_005640_218_2, acquired at $L_s = 347.4°$ (see fig. 1c). This means that the RSL had completely faded and had started lengthening again between the first two images (1a,b) and continued lengthening between $L_s = 331.5°$ and $L_s = 347.4°$. This is also confirmed by the analysis of HiRISE images of Hale crater in previous Martian Years reported by Stillman and Grimm (2018). In particular, from figure S9 of Stillman and Grimm (2018) we see that RSL lengthening occurs between $341.9° < L_s < 7°$ in MY 31 and $326.5° < L_s < 7°$ MY 32. This means that despite the HiRISE and CaSSIS images analyzed here being taken 30 days apart, the mechanisms responsible for RSL lengthening are active during this period and any seasonal fading can be considered negligible, allowing us to compare RSL albedos between the two images. In the following sections we will describe our dataset, summarized in figure (2), which combines HiRISE (section 2.1), CaSSIS (section 2.2) and Thermal Emission Imaging System (THEMIS; Christensen et al. (2004)) (section 2.3) observations. Image IDs and observation details for each of the products we used are detailed in Appendix A.

2.1. HiRISE data

We used the latest publicly available HiRISE image of the central peak of Hale crater, ESP_058618_1445, acquired on 27 January 2019 at 14:06 Mars local time and with a $L_s = 331.5°$, as well as the corresponding HiRISE DTM and orthophoto of the region. The RED channel (McEwen et al., 2007) of the HiRISE image was

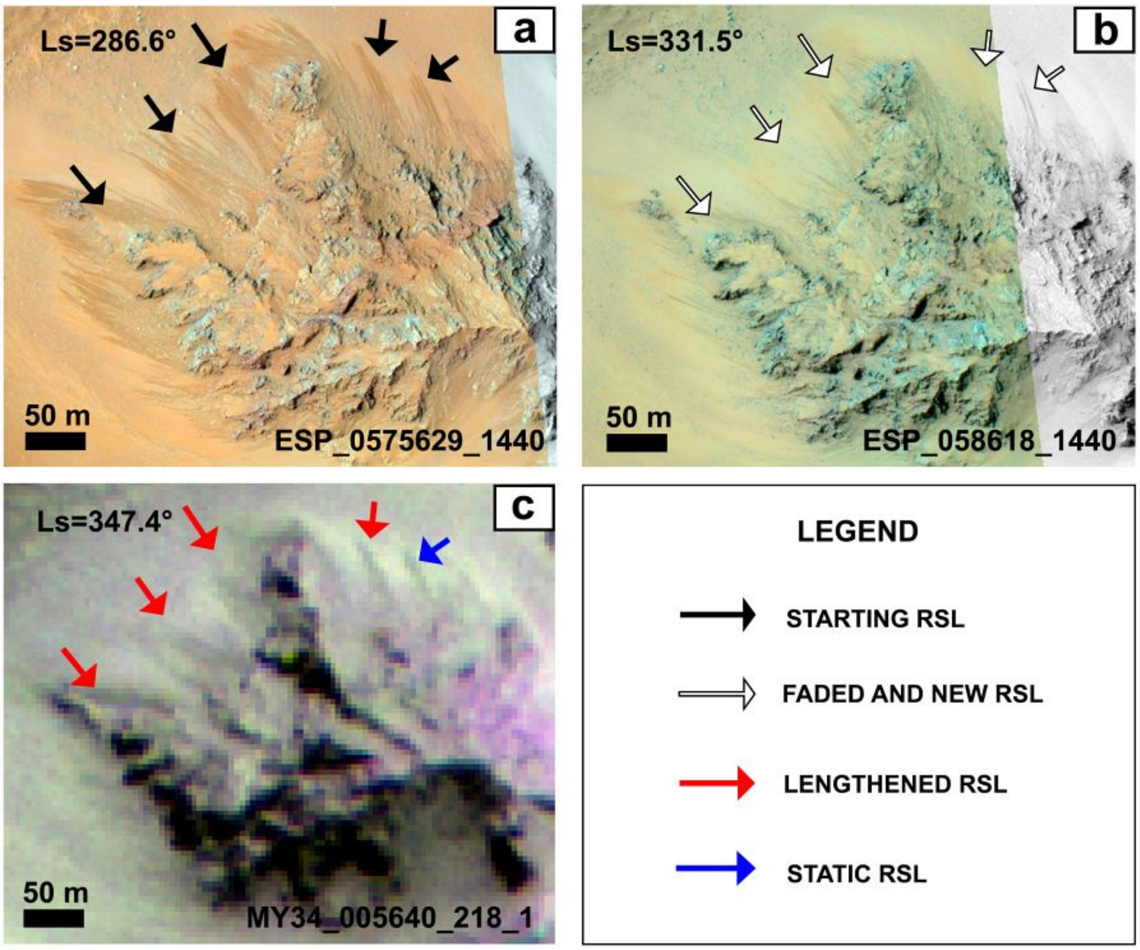

Figure 1: RSL activity during the 3rd pulse at Hale crater. a) HiRISE image showing areally extensive RSL, indicated by black arrows, at $L_s = 286.6°$. b) The same area but observed at $L_s = 331.5°$. White arrows indicate the same RSL in a) that faded and restarted their lengthening phase. c) Colour composite of the RED, PAN and BLU filters of CaSSIS image MY34_005640_218_2 taken at $L_s = 347.4°$ and showing that some a RSL in n) remained static (blue arrow) while others (red arrows) further lengthened with respect to the previous image. Areal extents of RSL in this area are mapped in figure (10).

orthorectified on the DTM using the NASA Ames Stereo Pipeline (Moratto et al., 2010). To obtain reliable slope and aspect measurements, we adapted the technique of Schaefer et al. (2019) to reduce noise and systematic artifacts present in the DTM and calculated slope and aspect maps using ArcGIS (Burrough and McDonell, 1998). In particular, the DTM was resampled at 2m resolution and smoothed with a 10 m radius moving average as in (Schaefer et al., 2019). The aligned HiRISE DTM, image, aspect and slope maps are shown in figure (2). More details about the HiRISE data products used in the analysis are provided in Appendix A.

2.2. CaSSIS data

The central peak of Hale crater was imaged by CaSSIS on 26 February 2019 at 11:13 Mars local time, with a $L_s = 347.4°$, in stereo mode and with the near infrared (NIR), red (RED), panchromatic (PAN) and blue (BLU) filters (Thomas et al., 2017). From the CaSISS stereo pair MY34_005640_218_1, a DTM and radiometrically calibrated orthophoto of the PAN channel of the second image in the stereo pair (i.e. MY34_005640_218_2) were obtained using the 3DPD photogrammetric pipeline described in Simioni et al. (2017). The CaSSIS orthophoto was then manually co-registered to the aligned HiRISE dataset in ArcGIS. The footprint of the CaSSIS stereo pair is shown in figure (2b) and a color composite image obtained by combining the overlap of the RED, PAN and BLU channels is shown in figure (2c).

2.3. THEMIS data

We used the MARSTHERM web interface (Putzig et al., 2013) to process THEMIS infrared observations within $\pm$ 5° of L_s of the CaSSIS image and derive thermal in-

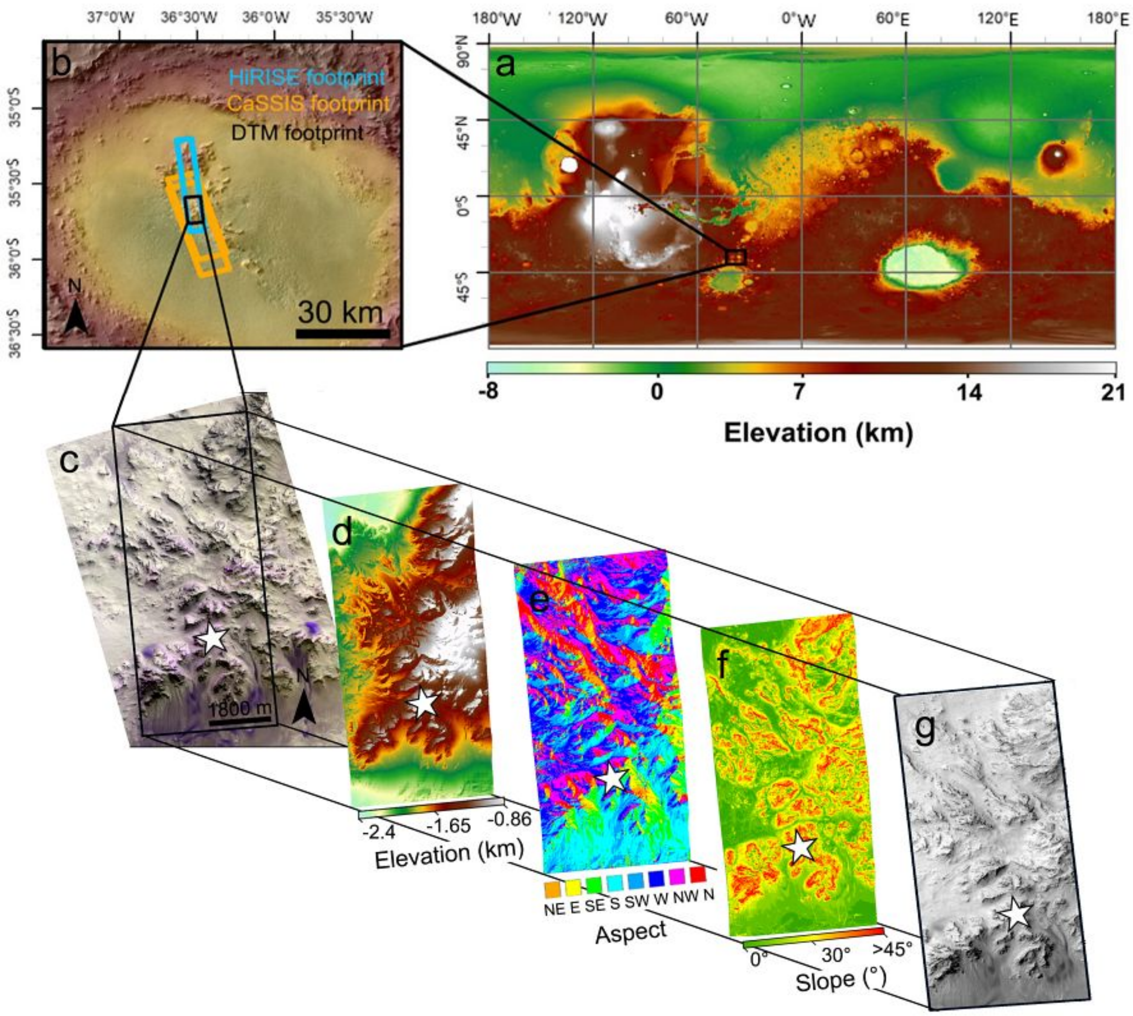

Figure 2: Schematic description of our dataset. a) Mars Orbiter Laser Altimeter (MOLA) colorized elevation map of Mars showing the location of Hale crater (black rectangle). b) MOLA colorized elevation map overlaid on THEMIS infrared daytime mosaic showing the central peak of Hale crater and the footprints of our observations. c) RGB color composite of the RED, PAN and BLU filters of CaSSIS image MY34_005640_218_2 depicting the central peak of Hale crater. d) HiRISE DTM, e) aspect and f) slope maps generated from the HiRISE DTM and g) HiRISE image ESP_058618_1445 projected onto the HiRISE DTM.The white star indicates the location of figure (1).

ertia maps of Hale crater at 100 m resolution. As is customary for Martian thermal modeling studies (Edwards and Piqueux, 2016; Fergason et al., 2006), we considered only nighttime observations. The final thermal inertia map was obtained by computing the median thermal inertia value at each pixel from all the selected observations. The thermal inertia map was then used to simulate surface and subsurface temperatures at Hale crater, as described in section (3.3).

3. Methods

3.1. General properties

We first identified all RSL that were resolved in both the HiRISE and CaSSIS images. Sometimes the RSL identified on the HiRISE image occurred in clusters of several lineae, spanning multiple CaSSIS pixels, but separated by distances lower than the CaSSIS resolution. In these cases we did not consider the single RSL, not resolved by CaSSIS, but the whole cluster. We mapped the envelope of each RSL, or cluster of RSL, in both images. To better compare the two images and cross-check any detected lengthening, we also resampled the HiRISE image at the CaSSIS resolution by summing all HiRISE pixels within a CaSSIS pixel and mapped the RSL envelopes on the resampled image. Examples of "changed" and "static" RSL, including their mapped envelopes are seen in figure (3). If a significant RSL lengthening could be detected using both the original and resampled images, we labeled the RSL as "changed", otherwise as "static". To take into account uncertainties in the comparison from any residual misalignment and/or differences in resolution and illumination between the two images, we considered a lengthening to be statistically robust only if greater than 1 CaSSIS pixel. This threshold is much lower than the typical lengthening that should occur between the two images, $\sim 60-100$ m given the average RSL advance rates (Levy, 2012; Stillman et al., 2016). To distinguish darkening caused by illumination conditions (i.e. topographic shading) from real RSL in the CaSSIS image we also considered the relative orientation between the slopes and the direction of the Sun, and avoided comparison of albedo features within highly shaded regions. Finally, we measured the mean slope and aspect at the termination point of every mapped RSL in the HiRISE image.

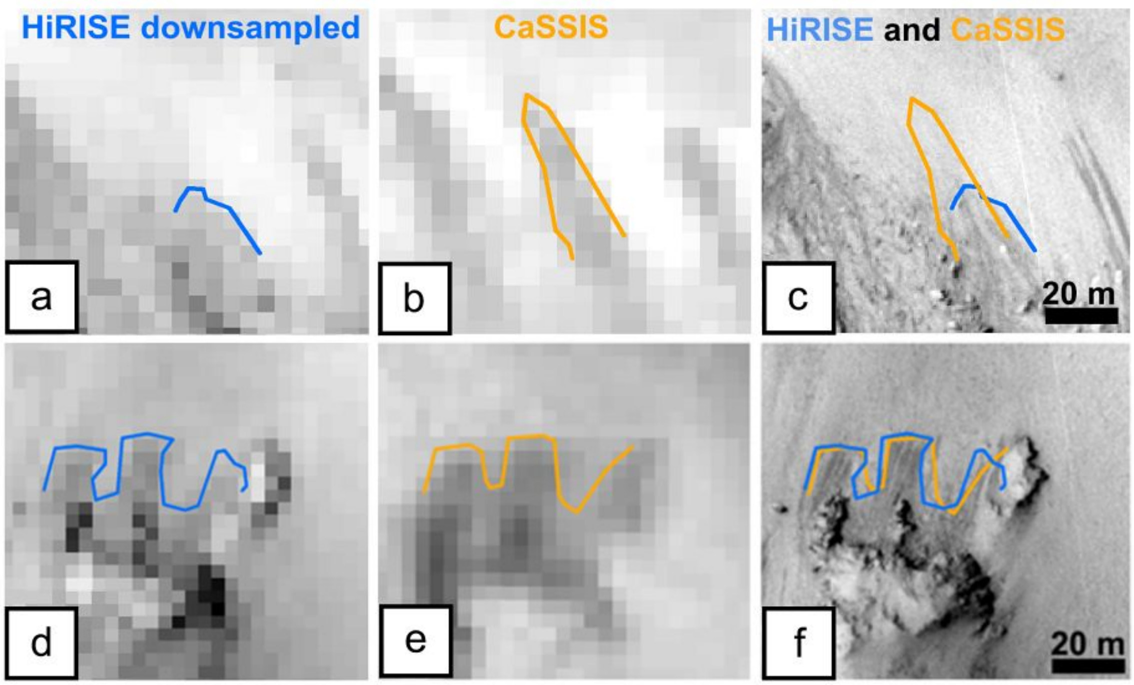

Figure 3: Examples of “changed” (upper row) and “static” (lower row) RSL envelopes mapped in blue on the downsampled afternnon HiRISE image (a,d) and in orange on the morning CaSSIS image (b,e). Panels (c) and (f) Show their comparison on top of the original HiRISE image.

3.2. Relative albedo

The relative albedo is the ratio between the reflectance (I/F) of two atmospherically corrected regions of the surface that have the same illumination conditions (Daubar et al., 2016). Our goal is to assess if RSL are darker, and thus potentially wetter, in the morning with respect to the afternoon. We compute the RSL relative albedo as the ratio between the reflectance of an RSL region and the reflectance of a nearby RSL-free region with the same illumination conditions, that is assumed to not have "changed". We only compare the CaSSIS PAN channel with the HiRISE RED channel. As these two filters closely correspond one to each other, the consistency between HiRISE and CaSSIS measurements is granted (Thomas et al., 2017). A complete multi-band analysis taking into account for differences between the CaSSIS RED and NIR and the HiRISE IR filters is left for a future work. In order to perform relative albedo measurements, it is necessary to first identify regions with similar slope and aspect, and in turn similar incidence angles. To do this, we first selected a set of regions of interest (ROI) from the previously identified RSL in both images (RSL ROI). To ensure that each RSL ROI is dominated by RSL signal, we used the HiRISE image for the selection and kept that same ROI in the CaSSIS image. Their mean slope and aspect were measured using ArcGIS. For each RSL ROI, we defined a corresponding background (BK) ROI in a nearby region, with similar mean slope and aspect but without RSL in either images. Where a suitable BK ROI could not be found, we did not include the RSL in the relative albedo analysis. This criterion proved to be the most restrictive, resulting in a relatively low number of suitable ROIs for relative albedo measurement, as discussed in section

(4.2). Figure (4) shows examples of some selected ROIs. We extracted the mean I/F and its standard deviation for each BK and RSL ROI and applied a first order atmospheric correction by subtracting the I/F value of the darkest pixel within shadows in the overlapping region of the two images from IF_{RSL}. To take into account the different resolutions of the two images, for HiRISE we used the mean I/F in a 4.6×4.6 m square area around the darkest pixel within shadows. Although this kind of atmospheric correction can be inaccurate in steep topography, it is often adopted when performing relative photometry (Daubar et al., 2016; Schaefer et al., 2019). In addition, more precise use of shadows areas for this purpose could be performed if required (Hoekzema et al., 2011). In our case, however, we only apply the atmospheric correction to the RSL ROIs and not to the BK ones. The rationale behind this approach is to take into account the non-linear effect of aerosols on the apparent reflectance of a surface, meaning that low-albedo surfaces are more brightened by diffuse light than high albedo ones (Vincendon et al., 2007). We finally computed the relative albedo as:

$$RA_* = \frac{IF_{RSL} - IF_D}{IF_{BK}} \qquad * \in \{H, C\} \tag{1}$$

where RA_* is the RSL relative albedo, computed either from the original HiRISE ($* = H$) or CaSSIS ($* = C$) images. IF_{RSL} is the mean I/F extracted from an RSL ROI. IF_D is the I/F of the darkest shadowed pixel and IF_{BK} is the I/F of a BK ROI. We compute uncertainties for the HiRISE and CaSSIS relative albedos applying standard error propagation (see Appendix B). The significance of any difference between the HiRISE and CaSSIS relative albedos is established applying standard statistical tests. We use the Kolmogorov-Smirnov (KS, Massey (1951)) and Wilcoxon (W, Wilcoxon (1945)) signed-rank statistical tests to assess if the HiRISE and CaSSIS relative albedos are sampled from the same distribution. We apply the Anderson-Darling (AD, Anderson and Darling (1954)) and Shapiro-Wilk statistical tests (SW, Shapiro and Wilk (1965)) to assess if the differences between the two distributions are stochastic. From each test, a $p-$value is computed and compared with the customary 0.05 threshold. All tests and the $p-$value computations are performed using routines implemented in the `nortest` library (Gross and Ligges, 2015) (`https://CRAN.R-project.org/package=nortest`) of the R programming language (R Core Team, 2019).

3.3. Thermal analysis

We simulated diurnal surface and subsurface temperatures on the region depicted in figure (5a) at the time of the CaSSIS observation using the thermal model of Schorghofer et al. (2019). This model solves the 1D thermal balance and diffusion equations in a rough surface, taking into account the contribution of 3D topography to the surface energy balance. Examples of modeled diurnal surface and subsurface temperature maps are shown in figure (6). We focused only on this region because it hosts many large RSL on multiple slope orientations and allowed us to reduce computation time. Within this region we defined different study zones, as depicted in figure (5b). To account for the different thermal behavior of different materials within our region, we distinguished between zones composed of exposed bedrock (i.e. those starting with “B” in figure (5d) and zones composed of finer material, like regolith (i.e. those starting with “S” in figure (5d)). For the former we estimate a

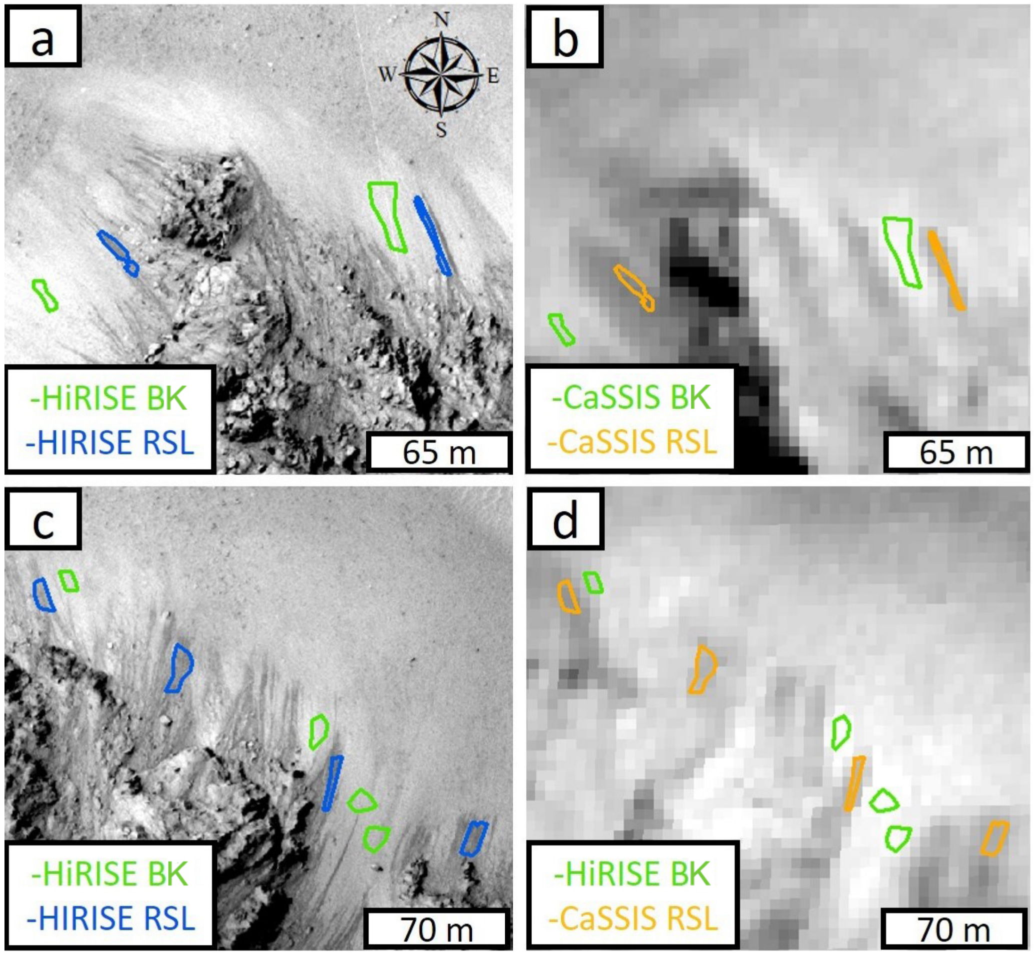

Figure 4: a,c): examples of RSL ROI (blue) and BK ROI (green) used to extract the mean I/F of RSL and RSL-free regions and their uncertainty from the HiRISE image. b,d): examples of RSL (orange) and BK (green) ROIs used to extract the mean I/F of RSL and RSL-free regions and their uncertainty from the CaSSIS orthoimage.

mean thermal inertia of 772^{+188}_{-130} TIU, and for the latter we estimate a mean thermal inertia of 540^{+128}_{-122} TIU (TIU is thermal inertia units, i.e. J m^{-2} s$^{-0.5}$ K^{-1}). Thermal inertia and 3σ uncertainties were estimated by computing the mean, maximum and minimum values of pixels within the "BEDROCK" and "SLOPE" ROIs defined in the thermal inertia map and depicted in figure (5d). These estimates are used, along with a DTM of the region, to simulate the mean, maximum and minimum diurnal temperature profiles at the surface and at 10 and 20 cm depth, as in (Chevrier and Rivera-Valentin, 2012). Although the thermal model has already been validated by Schorghofer et al. (2019) at Palikir crater, we also checked that the simulated temperatures of our zones agreed with the nighttime THEMIS IR observation I59655010, acquired at a $L_s = 348.8°$, close to the CaSSIS image L_s. THEMIS surface temperatures were obtained using the `https://www.thmproc.mars.asu.edu` website and are reported in figure (9).

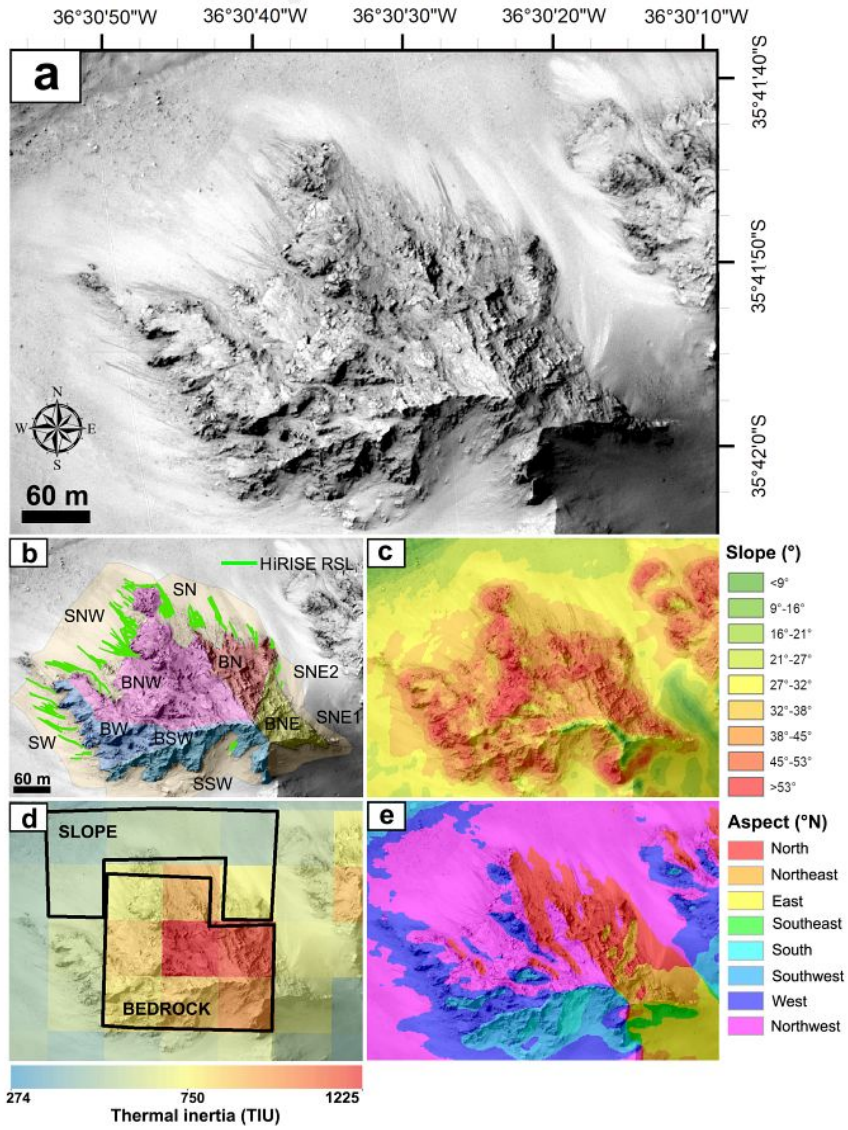

Figure 5: a) HiRISE image ESP_058618_1445 showing the selected region for the thermal analysis. b) Definition of zones where we simulated temperature profiles. c) Slope map. d) THEMIS-derived thermal inertia map. Black polygons represent the “BEDROCK” and “SLOPE” ROIs used to extract the thermal inertia of the bedrock material and the regolith, respectively. e) Aspect map.

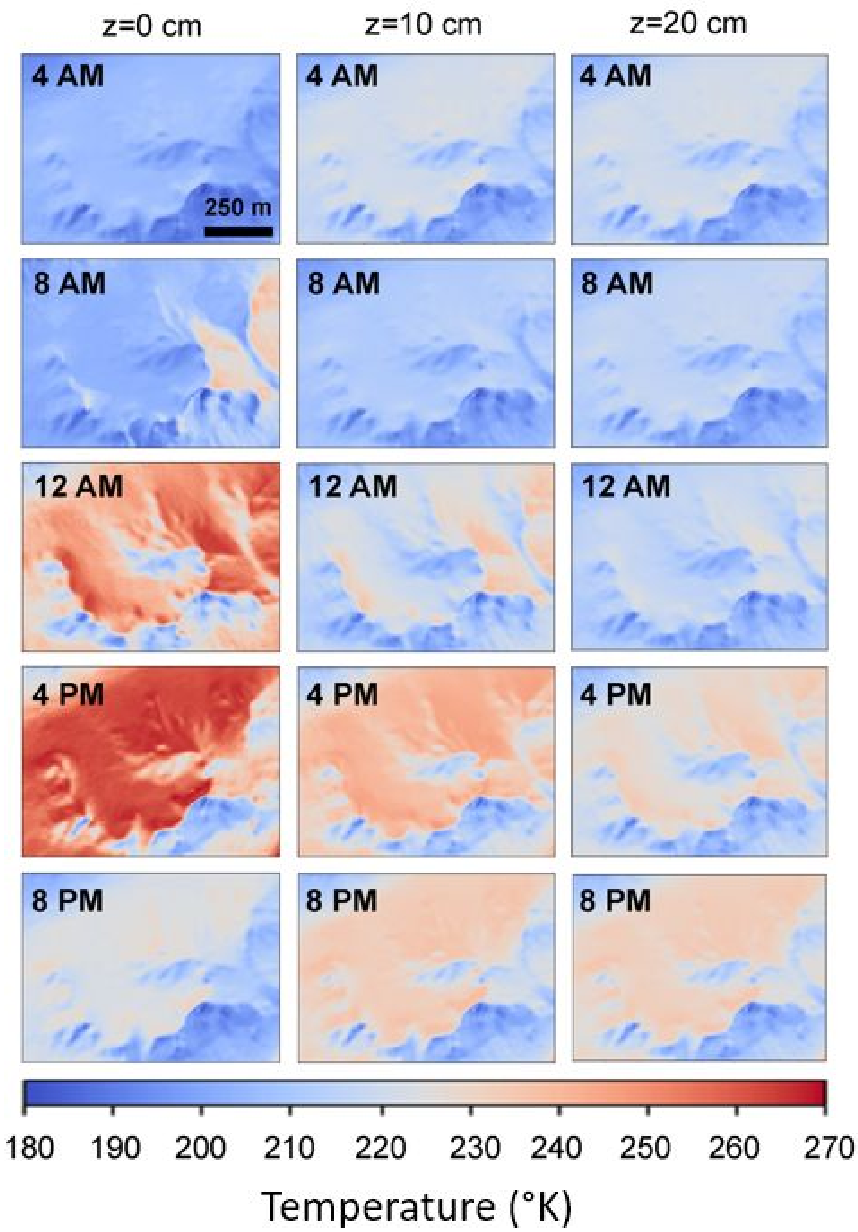

Figure 6: Example of diurnal temperature maps simulated at the surface (left), 10 cm depth (middle) and 20 cm depth (right). The simulations were performed using a THEMIS-derived thermal inertia of 770 TIU and used to extract diurnal temperature profiles for the bedrock.

4. Results

4.1. General properties

We identified 125 RSL, or groups of RSL in some cases, that were visible in both the HiRISE and CaSSIS images. Figures (7b,c and d) show examples of RSL as observed by CaSSIS. All the mapped RSL and their classification in terms of significant or absent lengthening between the morning and afternoon image are shown in figure (7a), while their slope and aspect distribution are in figures (8a,b) . In particular, the aspect distribution in figure (8b) shows that the considered RSL are found on north, north-west and west facing slopes and that there is no significant difference between the aspect of "static" and "changed" RSL. On the contrary, the slope distribution shows a dichotomy between the two classes. Most of the "static" RSL are found at slopes $< 30^\circ - 32^\circ$ while most of "changed" RSL are found at slopes $> 30^\circ - 32^\circ$.

4.2. Relative albedo analysis

We performed the relative albedo analysis on a selected sample of 11 RSL. The relatively low number of RSL considered for the relative albedo analysis is determined by the selection criteria discussed in section (3.2), i.e. we selected only RSL ROIs for which we could identify nearby BK ROIs having their same slope and aspect. In table (1) we report the CaSSIS (RA_C) and HiRISE (RA_H) RSL relative albedos, their difference and their 1σ uncertainties. We obtain average relative albedos of $\bar{R}A_H = 0.792 \pm 0.032$ for HiRISE and $\bar{R}A_C = 0.790 \pm 0.029$ for CaSSIS. These are broadly consistent with the relative albedo values measured by Schaefer et al. (2019) between

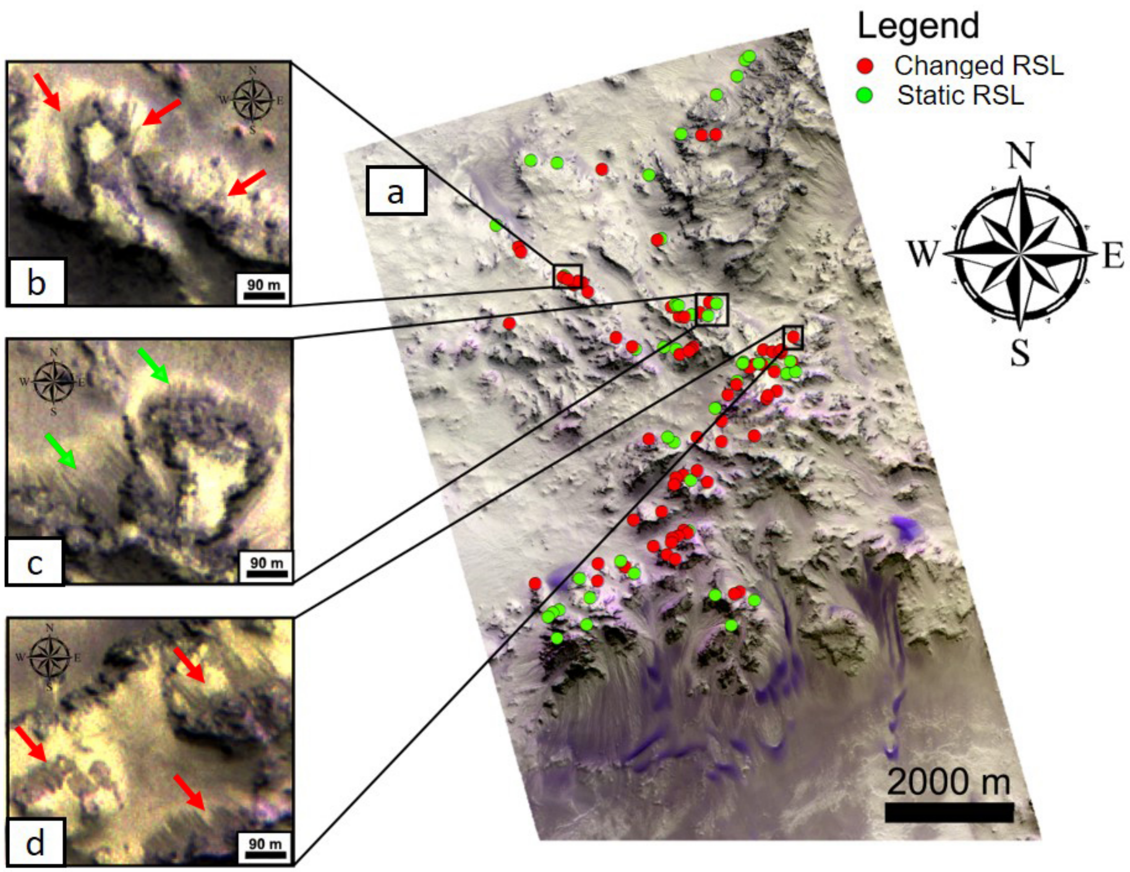

Figure 7: a) RGB color composite of the RED, PAN and BLU filters of CaSSIS image MY34_005640_218_2 depicting the central peak of Hale crater. Red dots indicate "changed" RSL. Green dots indicate "static" RSL. b), c) and d): examples of identified RSL, indicated by black arrows.

$L_s = 330°$ and $L_s = 343°$ at Tivat crater, prior to the fading of RSL, confirming that any possible seasonal pattern is not influencing our measurements. The RSL relative albedo values reported for each ROI in table (1) show that there are no significant differences between the HiRISE and CaSSIS observations. The uncertainty on the relative albedo differences in table (1) is given by the sum of the uncertainties on

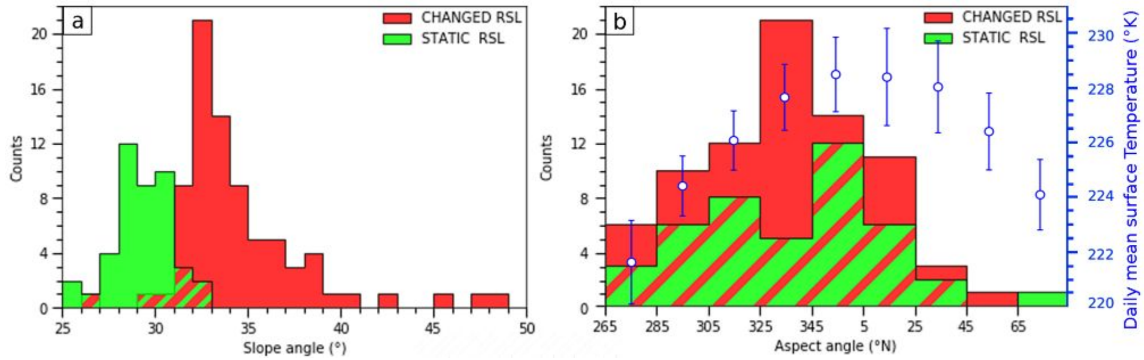

Figure 8: Distributions of a) slope and b) aspect of the termination points for “static” (green) and “changed” (red) RSL. The red-green striped part highlights where the two distributions overlap. The blue dots in b) are daily mean surface temperatures for each aspect bin for the region in figure (5). Error bars indicate the standard deviation within each aspect bin.

RA_C and RA_H and gives us an idea of the minimum albedo difference detectable by our methodology. We obtain a mean absolute uncertainty on $RA_C - RA_H$ of 0.09, corresponding to an average relative uncertainty of 11%. The relative albedo differences reported in table (1) are fully consistent with stochastic variability in the two datasets. To demonstrate this, we checked whether the differences between the HiRISE and CaSSIS relative albedos follow a normal distribution, applying both an Anderson-Darling and a Shapiro-Wilk test of normality. We obtained $p-$values of $P_{AD} = 0.48$ and $P_{SW} = 0.50$. These are greater than the customary $\alpha = 0.05$ threshold, so we cannot reject the null hypothesis that the relative albedo differences come from a normal distribution, i.e that they are stochastic. To further cross-check our results, we also applied a Kolmogorov-Smirnov and a Wilcoxon signed-rank test and assessed the hypothesis that the HiRISE and CaSSIS relative albedos are drawn from the same distribution. Both tests failed to reject the null hypothesis, resulting in $p-$values of $P_{KS} = 0.99$ and $P_W = 0.90$ both greater than the $\alpha = 0.05$ threshold,

ROI	RA_C	RA_H	$RA_C - RA_H$
1	0.76 ± 0.03	0.79 ± 0.06	-0.03 ± 0.09
2	0.73 ± 0.03	0.76 ± 0.05	-0.03 ± 0.08
3	0.79 ± 0.02	0.77 ± 0.06	0.02 ± 0.09
4	0.80 ± 0.02	0.75 ± 0.05	0.05 ± 0.07
5	0.78 ± 0.03	0.75 ± 0.05	0.03 ± 0.08
6	0.83 ± 0.04	0.80 ± 0.06	0.03 ± 0.10
7	0.82 ± 0.03	0.85 ± 0.06	-0.02 ± 0.08
8	0.76 ± 0.02	0.81 ± 0.08	-0.05 ± 0.10
9	0.83 ± 0.04	0.79 ± 0.06	0.04 ± 0.10
10	0.79 ± 0.02	0.79 ± 0.06	0.00 ± 0.08
11	0.81 ± 0.03	0.82 ± 0.07	-0.01 ± 0.10

Table 1: Relative albedo analysis results. RA_C and RA_H are the relative albedos of RSL with respect to nearby RSL-free slopes measured on CaSSIS and HiRISE images, respectively. $RA_C - RA_H$ is the difference between the CaSSIS and HiRISE relative albedo. Errors are reported as 1σ uncertainties.

confirming that the detected differences between the HiRISE and CaSSIS relative albedos are stochastic.

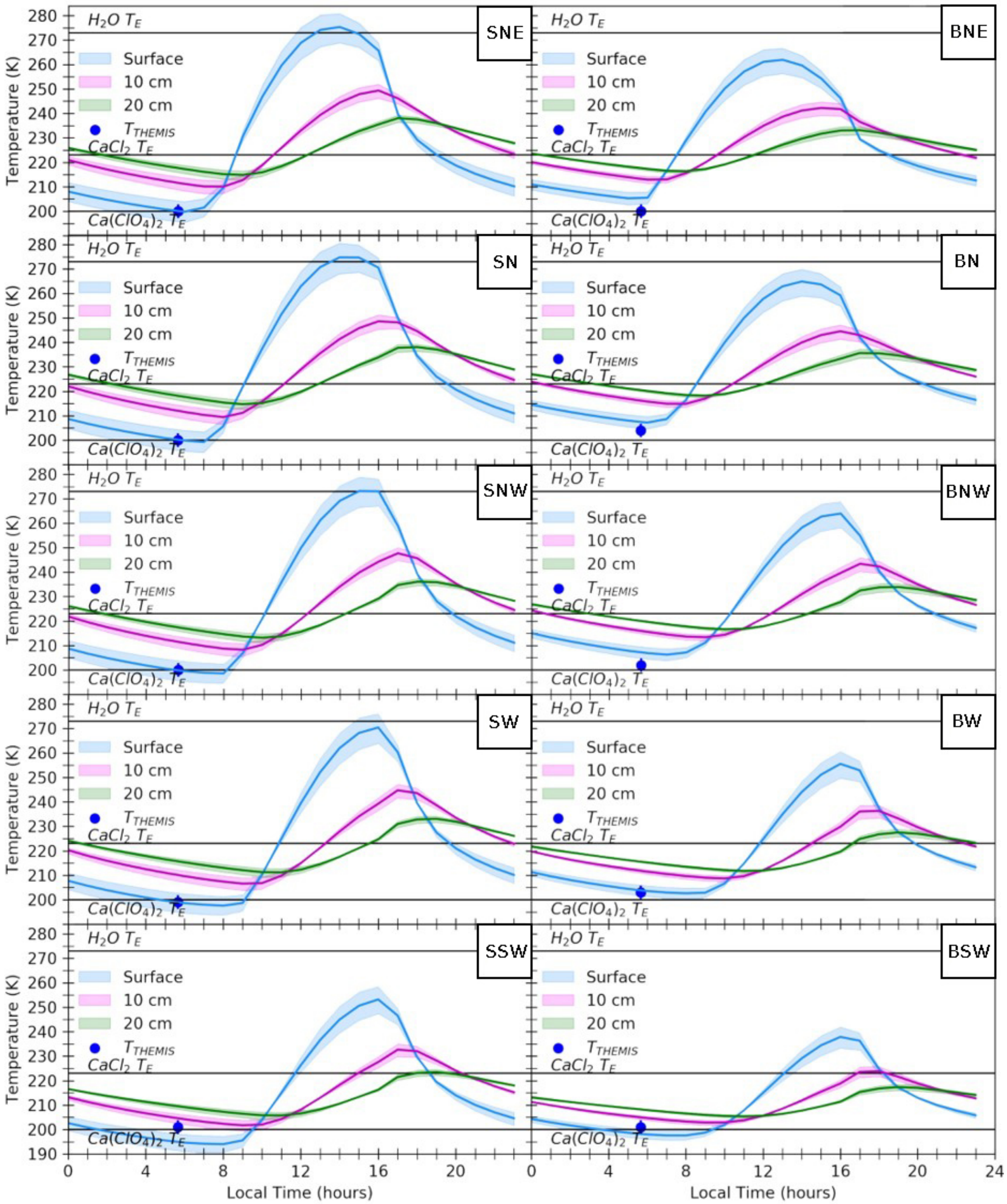

Figure 9: Diurnal temperature profiles (solid lines) with 3σ uncertainties (shaded areas) simulated at the surface (light blue), at 10 cm (magenta) and 20 cm depth (green) for the "Slope" (left) and "Bedrock" (right) ROIs defined in figure (5). Blue dots are mean THEMIS surface temperature of each ROI with 3σ uncertainties of 2.8 K (Fergason et al., 2006).

4.3. Thermal analysis

We simulated the thermal environment in a small region within Hale crater, shown in figure (5). Diurnal surface and subsurface temperature profiles and their uncertainties for each of the zones in figure (5) are shown in figure (9). In the same figures, we also show the eutectic temperatures of water ice, $CaCl_2$ brine (Gough et al., 2016) and Ca-perchlorate (Marion et al., 2010), as well as mean THEMIS surface temperatures for each ROI. From the temperature profiles in figures (9) we can see that both north-west, north and north-east regions transiently reach temperatures higher than the melting temperature of water ice only at the regolith surface, and not on bedrock or in the subsurface. In contrast, the transient melting of $CaCl_2$ or $Ca(ClO_4)_2$ frozen brines is generally supported in all these zones. In particular, from the temperature profiles in figure (9a) we see that north-east facing slopes allow the melting of $CaCl_2$ at 10 cm in the subsurface from $\sim$ 10:00 local time until $\sim$ midnight, and at 20 cm depth from $\sim$ 12:00 to $\sim$ 14:00. On north facing slopes (see figure (9b)) melting could occur from $\sim$ 11:00 to $\sim$ midnight at 10 cm depth and from $\sim$ 13:00 to $\sim$15:00 at 20 cm depth. On north-west facing slopes (see figure (9c)) melting happens from $\sim$ 12:00 until $\sim$ midnight at 10 cm depth and from $\sim$ 14:00 to $\sim$ 15:00 at 20 cm depth. West facing slopes (see figure (9d)) allow melting of from $\sim$ 13:00 until $\sim$ 23:00 local time at 10 cm depth, and from $\sim$ 15:00 to $\sim$ midnight at 20 cm depth. Finally, south-west facing slopes permit melting of $CaCl_2$ mostly on the regolith and from $\sim$ 15:00 to 20:00 at 10 cm depth. At 20 cm depth, temperatures are mostly below the eutectic temperature of $CaCl_2$ brines (see figure (9e)). In all these cases, melting of $Ca(ClO_4)_2$ is allowed at any hour of the day at all depths, except for north-west, west and south-west facing slopes where early morning surface temperatures are very close to 200 K and can reach values as low as 190K, below the eutectic temperature of this brine.

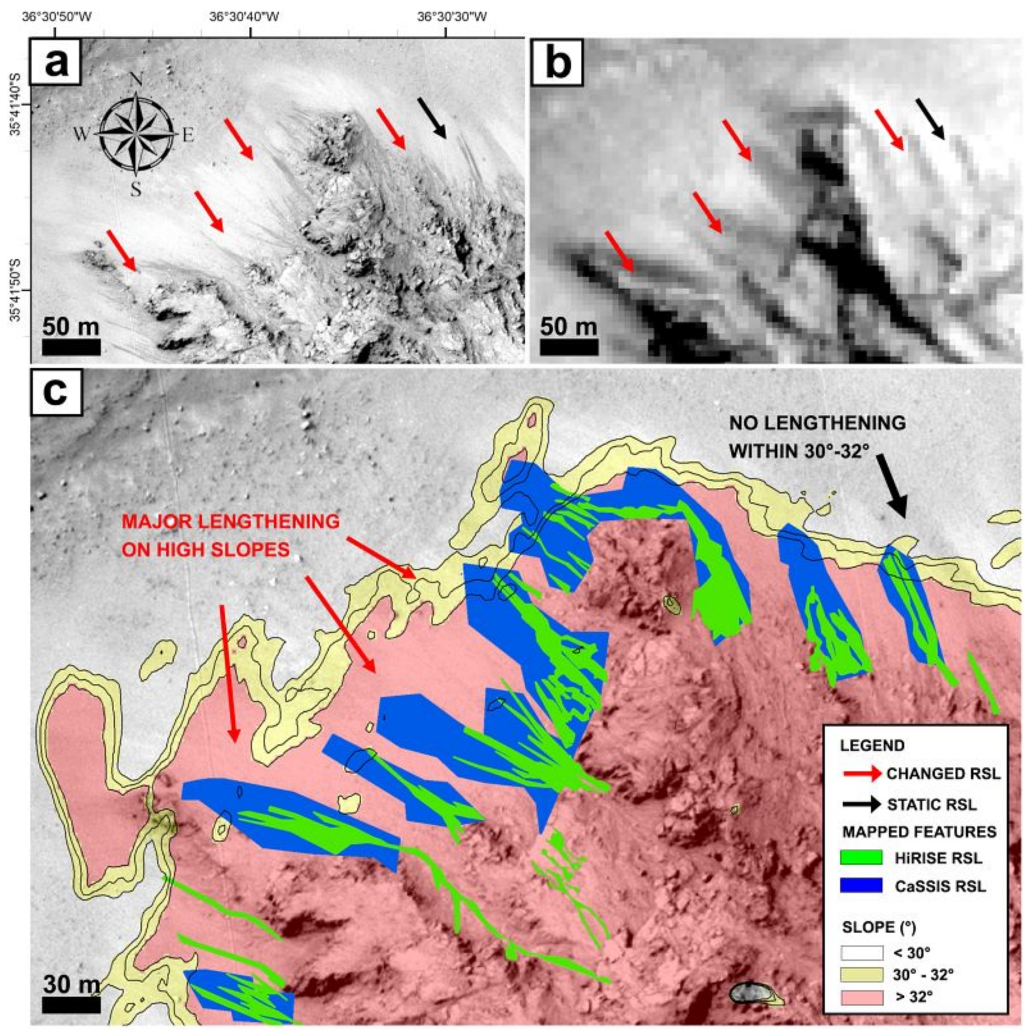

Figure 10: Mapping of HiRISE and CaSSIS RSL.a) HiRISE image depicting both "static" (black arrows) and "changed" RSL (red arrows) on the central peak of Hale crater. b) CaSSIS image showing the same RSL as in panel a). c) Mapping of HiRISE (green) and CaSSIS (blue) RSL overlain on a discretized slope map. The red part is where slopes are $> 32°$, the yellow part is for slopes between 30° and 32°.

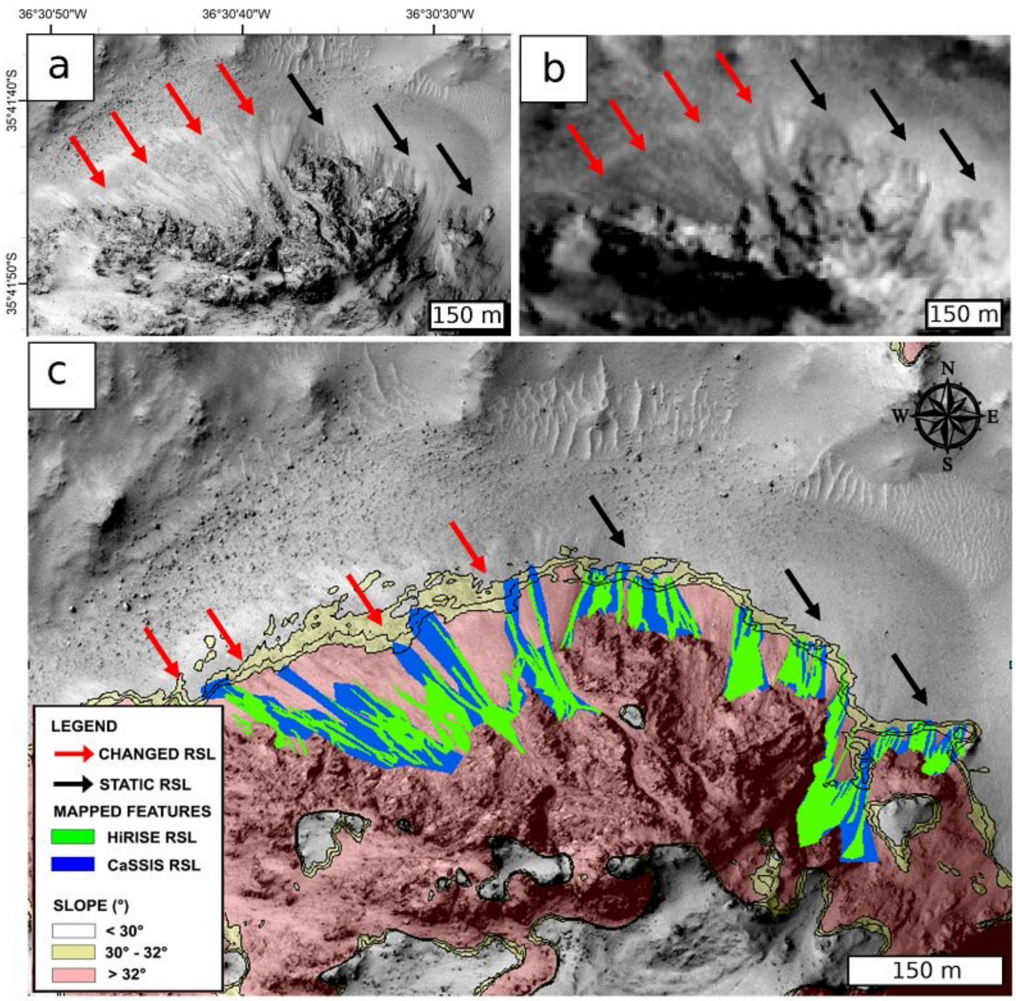

Figure 11: Mapping of HiRISE and CaSSIS RSL.a) HiRISE image depicting both "static" (black arrows) and "changed" RSL (red arrows) on the central peak of Hale crater. b) CaSSIS image showing the same RSL. c) Mapping of HiRISE (green) and CaSSIS (blue) RSL overlain on a discrete slope map. The red part is where slopes are > 32°, the yellow part is for slopes between 30° and 32°.

5. Discussion

Since at Hale we observe RSL starting on bedrock outcrops (figure (10c)), which generally have lower temperatures than the freezing point of water ice but higher than the considered brines, the latter are more likely than flows of seeping water. Moreover, exposed water ice is not predicted to form on equator-facing slopes at latitudes comparable to that of Hale crater (Schorghofer et al., 2019), and it is not observed by spectral instruments sensitive to micrometer-thick surfaces of water frost (Vincendon et al., 2010). Liquid brines may form via a) melting of a subsurface reservoir or b) deliquescence of salts. In the first case, either a reservoir near the surface or a subsurface deposit, which would be exposed by fractures, are necessary. The fractured rocky outcrops in the central peak of Hale crater might host these shallow brine reservoirs. In such a case, brine melting would occur when subsurface temperatures rise above their eutectic temperature, i.e. from mid-afternoon to evening hours, depending on its depth and slope orientation. This is because ice is more likely to be found in the shallow subsurface than at the surface at these latitudes. In particular, our thermal analysis suggests that melting of $CaCl_2$ brines should be favored on north-east, followed by north, north-west, west and south-west facing slopes. Melting of $Ca(ClO_4)_2$ brine is generally possible on all slopes, as it can occur over most of a Martian day. However north-east, north and north-west facing slopes are favored since their subsurface temperature is always higher than 200K at $L_s = 347.4°$. This can also be explained by considering the dependence of daily mean surface temperature from the slope aspect, depicted in figure (8). This predicts that north-east, north and north-west facing slopes have the highest daily mean surface temperatures. As a consequence, brines melting is favoured on these slopes. This picture hence suggests that if RSL are formed through melting of shallow subsurface brines, they should form and lengthen from noon and early-afternoon to evening hours favouring north-east, north and north-west facing slopes.

In the case of deliquescence, the main parameters constraining RSL activity are surface temperature and relative humidity. As shown in figure (9) surface temperatures are above the eutectic temperature of $CaCl_2$ from $\sim$ 8:00 to $\sim$ 19:00-20:00 Mars local time, depending on the slope orientation and thermal inertia. However, the RH may not be high enough during these hours. In particular, (Steele et al., 2017) and (Fischer et al., 2019) show that from $\sim$ 8:00 to $\sim$ 19:00-20:00, RH values are below 5% both at Gale crater and at the Phoenix landing site during local summer. This makes perchlorates more interesting candidates, because surface temperatures are above their eutectic temperature at any time of day, except for north-west, west and south-west facing and slopes during early morning. If RSL are deliquescence-related features, we should see a similar aspect preference as that expected for the melting of brines, but more shifted towards north-east facing slopes. In fact, these slopes reach higher surface temperatures at earlier local times, at a time when air relative humidity is higher (Gough et al., 2016; Steele et al., 2017; Fischer et al., 2019), which enhances deliquescence. The aspect distribution in figure (8b) suggests quite a different picture, showing a preference for north, north-west and west facing slopes over north-east facing slopes. An example of this behavior is also illustrated in figures (10) and (11) where RSL sourcing from north-east facing slopes are fewer in number and less extensive than on north, north-west and even west facing slopes. This aspect distribution may be an indication that RSL lengthening is not associated with surface moisture, deliquescence of salts or melting of brines. Another option may instead be that deliquescence occurs during sunset instead of early morning when temperatures fall and relative humidity rises, as suggested by (Tebolt et al., 2020). In this case, west-facing, north-west and north facing slopes may be favoured as they have slightly higher evening surface temperatures, possibly explaining the aspect distribution at Hale crater. While this is in principle consistent with our aspect distribution, it is not supported by either laboratory experiments (Gough et al., 2016), REMS (Steele et al., 2017) or TECP data (Fischer et al., 2019), which suggest, instead, that early morning hours should be more favourable for deliquescence than evening hours.Moreover, it may not be in agreement with the very low water content of RSL estimated from nighttime IR observations (Edwards and Piqueux, 2016). Detailed, high-resolution modeling may be necessary to further explore the precise interplay between temperature and relative humidity at RSL locations and quantify the best periods for deliquescence. An indication that RSL at Hale crater may be dry flows is that their lengthening stops at slope angles $\sim 30°$ (Dundas et al., 2017). We also detect this behavior in our slope distribution in figure (8a) and in figures (10,11), which show that RSL lengthening is generally correlated with the presence of slopes steeper than $\sim 30° - 32°$. On the contrary, RSL that already reached slopes within this range or shallower remained static. This dichotomy is shown in figure (8a), where there is a significant difference between the "changed" and "static" slope distributions. This dichotomy is expected for dry flows that stop when they reach the angle of repose, producing the observed sample of "static" RSL, and lengthen on steeper slopes, producing the observed sample of "changed" RSL. In one case, we also detect a RSL that lengthened at a slope angle of $\sim 26°$. A similar behaviour has also been detected by Stillman et al. (2020) and Tebolt et al. (2020). Although, in principle, this would support wet-based flows, the fact that they occur with a very low frequency suggests that these RSL could be statistical outliers (Stillman et al., 2020). As such, it is possible that additional and/or different mechanisms may be at play in this sample of RSL. Dedicated analyses considering statistically significant occurrences of these RSL and consideration of uncertainties in the DTM used for computing the slope values may be necessary to reach a definitive conclusion. Our comparison of HiRISE and CaSSIS RSL relative albedo indicates that there are no significant diurnal variations between 11:13 and 14:06 local time, a result expected for dry flows. However, it may be also possible that significant dehydration has already occurred at 11:13, producing the observed result independently from how RSL form, or that the relative albedo differences at play are lower than 11%. If RSL are formed through deliquescence, the importance of this issue depends on salt composition and its interaction with the regolith, as these both affect the DRH and ERH (efflorescence relative humidity) of the solution (Nuding et al., 2014). In particular, Nuding et al. (2014) showed that liquid $Ca(ClO_4)_2$ brines persist with very low RH values. Therefore, if liquid brines form on early morning they may persist until late morning in a metastable state and dehydrate during the afternoon. Again, detailed near-surface relative humidity modeling should be performed to determine whether these processes are occurring at RSL sites. Another interpretation of our relative albedo measurement, which is not supported by thermal studies (Edwards and Piqueux, 2016), is that the water supply exceeds evaporative losses. In this case dehydration does not occur and there is no significant albedo variation (Hillel, 2004). Future observations acquired during early morning will help to better characterize the diurnal albedo of RSL. Nevertheless, the relative albedo measurements reported here could provide a useful validation for modeling and experimental studies of RSL.

In summary, our result collectively support dry flows as responsible for RSL lengthening. The triggering mechanisms which initiate these flows may involve thermal creep (Schmidt et al., 2017; Schaefer et al., 2019), or aeolian processes (Vincendon et al., 2019). In particular, the latter would also be able to describe the temporal evolution of RSL activity during the third pulse shown in figure (1) (Vincendon et al., 2019). While our results support dry flows models, brines and more generally volatiles may still play and indirect and concurrent role in RSL formation by triggering dry mass fluxes (Massé et al., 2016; Wang et al., 2019; Bishop et al., 2019), but our data does not provide any additional insight on RSL triggering.

6. Summary and Conclusions

We presented the first CaSSIS observation of RSL obtained during local morning at Hale crater, Mars. We identified a set of 125 RSL and studied their overall morphology, slope and aspect distributions and analyzed their thermal environment. We performed an initial comparison of their relative albedo using morning CaSSIS and afternoon HiRISE observations. Our comparison of RSL, as viewed through HiRISE and CaSSIS, 30 days later, reveals that most RSL lengthening occurred where slopes $> 30^\circ - 32^\circ$ were available. Instead, RSL on slopes $> 30^\circ - 32^\circ$ remained generally static. This result supports a dry granular flow dynamics, as suggested by other authors (Dundas et al., 2017; Vincendon et al., 2019; Schaefer et al., 2019; McEwen et al., 2019). The simulated diurnal surface and subsurface temperature profiles at Hale crater suggest that melting of brines and deliquescence of salts would be both favoured on north-east facing slopes, followed by north and north-west facing slopes. However, this pattern is different from our observed aspect distribution of "changed" RSL at Hale crater, suggesting that RSL lengthening is not controlled by surface moisture, deliquescence of salts or melting of brines. We compared HiRISE and CaSSIS RSL relative albedo between 11:13 and 14:06 local time, respectively, and found no significant differences, another result expected for dry flows. Our measurements could provide a useful validation for future models and experimental studies on RSL formation and lengthening. We conclude that the RSL at Hale crater are best explained as dry flows, in agreement with the conclusions of other authors (Dundas et al., 2017; Vincendon et al., 2019; Schaefer et al., 2019; McEwen et al., 2019). These may be triggered through thermal creep (Schmidt et al., 2017; Schaefer et al., 2019), aeolian processes (Vincendon et al., 2019), or very limited brine activity (Massé et al., 2016; Wang et al., 2019; Bishop et al., 2019). Future CaSSIS observations of RSL sites acquired earlier in the morning, in combination with same-day afternoon HiRISE images, will be pivotal in improving the characterization of the diurnal activity of RSL and will provide a clearer picture of their formation mechanism.

7. Acknowledgments

We would like to thank Dr. Mathieu Vincendon and Dr. Mauro Spagnuolo for their important and constructive comments that led to a great improvement of the manuscript. The authors also wish to thank the spacecraft and instrument engineering teams for the successful completion of the instrument. CaSSIS is a project of the University of Bern and funded through the Swiss Space Office via ESA's PRODEX programme. The instrument hardware development was also supported by the Italian Space Agency (ASI) (ASI-INAF agreement no.I/018/12/0), INAF/Astronomical Observatory of Padova, and the Space Research Center (CBK) in Warsaw. Support from SGF (Budapest), the University of Arizona (Lunar and Planetary Lab.) and NASA are also gratefully acknowledged. The relative albedo measurement presented in table (1) can be found online at `http://doi.org/10.5281/zenodo.3591990`. The study has been supported by the Italian Space Agency (ASI-INAF agreement no. 2017-03-17). SJC acknowledges the French Space Agency CNES for supporting her HiRISE and CaSSIS related work.

Declaration of competing interest

The authors declare that they have no known competing financial interests or personal relationships that could have appeared to influence the work reported in this paper

Appendix

In Appendix A we report some details of the products used for the analysis, such as image IDs, resolution, solar longitude, local solar time, incidence, emission and phase angles. In Appendix B we show details on the error propagation for computation of relative albedo uncertainties.

Appendix A. Dataset details

We report in table (A.2) some details on the data products defined in section (2) of the main text.

Product type	ID	Resolution m	L_s (°)	LTST hh:mm	Incidence (°)	Emission (°)	Phase (°)
HiRISE orthoimage	ESP_031203_1440_RED_C_01_ORTHO	0.25	287.7	14:40	37.0†	13.9†	23.5†
HiRISE Image	ESP_058618_1445_RED	0.50	331.5	14:06	37.0	4.0	40.7
HiRISE DTM	DTEEC_030715_1440_030570_1440_A01	1.00					
CaSSIS stereo image 1	MY34_005640_218_1	4.65	347.4	11:13	32.8	11.4	23.4
CaSSIS stereo image 2	MY34_005640_218_2	4.65	347.4	11:13	32.8	10.6	40.1
THEMIS IR image	I01144003	100.00	344.1	03 : 18	119.1	0.7	118.7
THEMIS IR image	I59655010	100.00	348.4	05 : 40	84.6	1.9	84.4
THEMIS IR image	I67826009	100.00	341.1	06 : 30	91.2	0.7	91.1

Table A.2: Summary of the products used in the analysis. Solar longitude (L_s), Local time (LTST), incidence, emission and phase angles are taken from `https://www.uahirise.org` for HiRISE, and from `http://viewer.mars.asu.edu/` for THEMIS. †The reported incidence, emission and phase angle refers to the corresponding HiRISE Reduced Data Record (RDR) product.

Appendix B. Relative albedo uncertainty

We defined the relative albedo (see text for details) as:

$$RA_* = \frac{IF_{RSL} - IF_D}{IF_{BK} - IF_D} \qquad * = H, C \tag{B.1}$$

where RA_* is the RSL relative albedo and $*$ is H for HiRISE and C for CaSSIS. IF_{RSL} is the mean I/F extracted from an RSL ROI. IF_D is the I/F of the darkest shadowed pixel and IF_{BK} is the I/F of a BK ROI. To compute the uncertainties in our relative albedo measurements, we used a standard error propagation approach. In particular, we performed the following approximation:

$$\sigma_{IF_{RSL}-IF_D} \sim 2 \cdot \sigma_{IF_{RSL}} \tag{B.2}$$

$$\sigma_{IF_{BK}-IF_D} \sim 2 \cdot \sigma_{IF_{BK}} \tag{B.3}$$

where $\sigma_{IF_{RSL}-IF_D}$ and $\sigma_{IF_{RSL}-IF_D}$ are the uncertainties of the numerator and denominator of equation (B.1). This approximation is justified for two reasons: first, we do not have an unambiguous way to define a ROI within shadows in and retrieve its mean flux and its standard deviation. Second, we do not know the errors on the HiRISE or CaSSIS radiometric calibration equations and thus we cannot propagate the uncertainty on the Digital Number (DN) of the darkest shadowed pixel. Instead, we can reasonably expect its uncertainty to be of the same order of magnitude as the uncertainty in IF_{RSL} and IF_{BK}. With this approximation, the uncertainty on relative albedo measurements may be propagated as:

$$\sigma_{A_*} = \sqrt{\left(\frac{\partial A_*}{\partial(IF_{RSL} - IF_D)}\sigma_{IF_{RSL}-IF_D}\right)^2 + \left(\frac{\partial A_*}{\partial(IF_{BK} - IF_D)}\sigma_{IF_{BK}-IF_D}\right)^2} =$$

$$= A_* \sqrt{\left(\frac{2\sigma_{IF_{RSL}}}{IF_{RSL} - IF_D}\right)^2 + \left(\frac{2\sigma_{IF_{BK}}}{IF_{BK} - IF_D}\right)^2}$$

References

A. Z. Abotalib and E. Heggy. A deep groundwater origin for recurring slope lineae on Mars. *Nature Geoscience*, 12:235–241, Mar. 2019. doi: 10.1038/s41561-019-0327-5.

T. W. Anderson and D. A. Darling. A test of goodness of fit. *Journal of the American Statistical Association*, 49(268):765–769, 1954. doi: 10.1080/01621459.1954.10501232.

J. L. Bishop, J. D. Toner, P. Englert, V. C. Gulick, A. S. McEwen, Z. F. M. Burton, M. F. Thomas, E. K. Gibson, and C. Koeberl. Salty Solution to Slipping Soils on Martian Slopes. In *Lunar and Planetary Science Conference*, Lunar and Planetary Science Conference, page 1188, Mar 2019.

P. A. Burrough and R. A. McDonell. *Principles of Geographical Information Systems* . Oxford University Press, New York, 1998.

V. F. Chevrier and E. G. Rivera-Valentin. Formation of recurring slope lineae by liquid brines on present-day mars. *Geophysical Research Letters*, 39(21), 2012.

doi: 10.1029/2012GL054119. URL https://agupubs.onlinelibrary.wiley.com/doi/abs/10.1029/2012GL054119.

M. Chojnacki, A. McEwen, C. Dundas, L. Ojha, A. Urso, and S. Sutton. Geologic context of recurring slope lineae in melas and coprates chasmata, mars. *Journal of Geophysical Research: Planets*, 121(7):1204–1231, 2016. doi: 10.1002/2015JE004991. URL https://agupubs.onlinelibrary.wiley.com/doi/abs/10.1002/2015JE004991.

P. R. Christensen, B. M. Jakosky, H. H. Kieffer, M. C. Malin, J. McSween, Harry Y., K. Nealson, G. L. Mehall, S. H. Silverman, S. Ferry, M. Caplinger, and M. Ravine. The Thermal Emission Imaging System (THEMIS) for the Mars 2001 Odyssey Mission. *Space Sci. Rev.*, 110(1):85–130, Jan 2004. doi: 10.1023/B:SPAC.0000021008.16305.94.

I. J. Daubar, C. M. Dundas, S. Byrne, P. Geissler, G. D. Bart, A. S. McEwen, P. S. Russell, M. Chojnacki, and M. P. Golombek. Changes in blast zone albedo patterns around new martian impact craters. *Icarus*, 267:86–105, Mar 2016. doi: 10.1016/j.icarus.2015.11.032.

C. M. Dundas, A. S. McEwen, M. Chojnacki, M. P. Milazzo, S. Byrne, J. N. McElwaine, and A. Urso. Granular flows at recurring slope lineae on Mars indicate a limited role for liquid water. *Nature Geoscience*, 10(12):903–907, Dec 2017. doi: 10.1038/s41561-017-0012-5.

C. S. Edwards and S. Piqueux. The water content of recurring slope lineae on

Mars. *Geophysical Research Letters*, 43(17):8912–8919, Sep 2016. doi: 10.1002/2016GL070179.

R. L. Fergason, P. R. Christensen, and H. H. Kieffer. High-resolution thermal inertia derived from the Thermal Emission Imaging System (THEMIS): Thermal model and applications. *Journal of Geophysical Research (Planets)*, 111(E12):E12004, Dec 2006. doi: 10.1029/2006JE002735.

E. Fischer, G. M. Martínez, N. O. Rennó, L. K. Tamppari, and A. P. Zent. Relative humidity on mars: New results from the phoenix tecp sensor. *Journal of Geophysical Research: Planets*, 124(11):2780–2792, 2019. doi: 10.1029/2019JE006080. URL https://agupubs.onlinelibrary.wiley.com/doi/abs/10.1029/2019JE006080.

R. V. Gough, V. F. Chevrier, and M. A. Tolbert. Formation of liquid water at low temperatures via the deliquescence of calcium chloride: Implications for Antarctica and Mars. *Planet. Space Sci.*, 131:79–87, Oct 2016. doi: 10.1016/j.pss.2016.07.006.

R. E. Grimm, K. P. Harrison, and D. E. Stillman. Water budgets of martian recurring slope lineae. *Icarus*, 233:316 – 327, 2014. ISSN 0019-1035. doi: https://doi.org/10.1016/j.icarus.2013.11.013. URL http://www.sciencedirect.com/science/article/pii/S0019103513004764.

J. Gross and U. Ligges. *nortest: Tests for Normality*, 2015. URL https://CRAN.R-project.org/package=nortest. R package version 1.0-4.

D. Hillel. *Introduction to environmental soil physics.* Elsevier Sicence & Technology, 2004.

N. Hoekzema, M. Garcia-Comas, O. Stenzel, E. Petrova, N. Thomas, W. Markiewicz, K. Gwinner, H. Keller, and W. Delamere. Retrieving optical depth from shadows in orbiter images of mars. *Icarus*, 214(2):447 – 461, 2011. ISSN 0019-1035. doi: https://doi.org/10.1016/j.icarus.2011.06.009. URL http://www.sciencedirect.com/science/article/pii/S0019103511002181.

C. Huber, L. Ojha, L. Lark, and J. W. Head. Physical models and predictions for Recurring Slope Lineae formed by wet and dry processes. *Icarus*, 335:113385, Jan 2020. doi: 10.1016/j.icarus.2019.07.019.

E. K. Leask, B. L. Ehlmann, M. M. Dundar, S. L. Murchie, and F. P. Seelos. Challenges in the Search for Perchlorate and Other Hydrated Minerals With 2.1-μm Absorptions on Mars. *Geophys. Res. Lett.*, 45(22):12,180–12,189, Nov 2018. doi: 10.1029/2018GL080077.

J. Levy. Hydrological characteristics of recurrent slope lineae on mars: Evidence for liquid flow through regolith and comparisons with antarctic terrestrial analogs. *Icarus*, 219(1):1 – 4, 2012. ISSN 0019-1035. doi: https://doi.org/10.1016/j.icarus.2012.02.016. URL http://www.sciencedirect.com/science/article/pii/S0019103512000644.

J. Levy, A. Nolin, A. Fountain, and J. Head. Hyperspectral measurements of wet, dry and saline soils from the McMurdo Dry Valleys: soil moisture properties from remote sensing. *Antarctic Science*, 26(5):565–572, Oct 2014. doi: 10.1017/S0954102013000977.

G. Marion, D. Catling, K. Zahnle, and M. Claire. Modeling aqueous perchlorate chemistries with applications to mars. *Icarus*, 207(2):675 – 685, 2010. ISSN 0019-1035. doi: https://doi.org/10.1016/j.icarus.2009.12.003. URL `http://www.sciencedirect.com/science/article/pii/S0019103509004904`.

M. Massé, S. J. Conway, J. Gargani, M. R. Patel, K. Pasquon, A. McEwen, S. Carpy, V. Chevrier, M. R. Balme, L. Ojha, M. Vincendon, F. Poulet, F. Costard, and G. Jouannic. Transport processes induced by metastable boiling water under Martian surface conditions. *Nature Geoscience*, 9(6):425–428, Jun 2016. doi: 10.1038/ngeo2706.

F. J. Massey. The kolmogorov-smirnov test for goodness of fit. *Journal of the American Statistical Association*, 46(253):68–78, 1951. ISSN 01621459. URL `http://www.jstor.org/stable/2280095`.

A. S. McEwen, E. M. Eliason, J. W. Bergstrom, N. T. Bridges, C. J. Hansen, W. A. Delamere, J. A. Grant, V. C. Gulick, K. E. Herkenhoff, L. Keszthelyi, R. o. L. Kirk, M. T. Mellon, S. W. Squyres, N. Thomas, and C. M. Weitz. Mars Reconnaissance Orbiter's High Resolution Imaging Science Experiment (HiRISE). *Journal of Geophysical Research (Planets)*, 112(E5):E05S02, May 2007. doi: 10.1029/2005JE002605.

A. S. McEwen, L. Ojha, C. M. Dundas, S. S. Mattson, S. Byrne, J. J. Wray, S. C. Cull, S. L. Murchie, N. Thomas, and V. C. Gulick. Seasonal flows on warm martian slopes. *Science*, 333(6043):740–743, 2011. ISSN 0036-8075. doi: 10.1126/science.1204816. URL `https://science.sciencemag.org/content/333/6043/740`.

A. S. McEwen, C. M. Dundas, S. S. Mattson, A. D. Toigo, L. Ojha, J. J. Wray, M. Chojnacki, S. Byrne, S. L. Murchie, and N. Thomas. Recurring slope lineae in equatorial regions of Mars. *Nature Geoscience*, 7(1):53–58, Jan 2014. doi: 10.1038/ngeo2014.

A. S. McEwen, E. Schafer, S. Sutton, and M. Chojnacki. Abundant Recurring Slope Lineae (RSL) Following the 2018 Planet-Encircling Dust Event (PEDE). In *Lunar and Planetary Science Conference*, Lunar and Planetary Science Conference, page 1376, Mar 2019.

Z. M. Moratto, M. J. Broxton, R. A. Beyer, M. Lundy, and K. Husmann. Ames Stereo Pipeline, NASA's Open Source Automated Stereogrammetry Software. In *Lunar and Planetary Science Conference*, volume 41 of *Lunar and Planetary Science Conference*, page 2364, Mar. 2010.

D. Nuding, E. Rivera-Valentin, R. Davis, R. Gough, V. Chevrier, and M. Tolbert. Deliquescence and efflorescence of calcium perchlorate: An investigation of stable aqueous solutions relevant to mars. *Icarus*, 243:420 – 428, 2014. ISSN 0019-1035. doi: https://doi.org/10.1016/j.icarus.2014.08.036. URL `http://www.sciencedirect.com/science/article/pii/S0019103514004527`.

L. Ojha, A. McEwen, C. Dundas, S. Byrne, S. Mattson, J. Wray, M. Masse, and E. Schaefer. Hirise observations of recurring slope lineae (rsl) during southern summer on mars. *Icarus*, 231:365 – 376, 2014. ISSN 0019-1035. doi: https://doi.org/10.1016/j.icarus.2013.12.021. URL http://www.sciencedirect.com/science/article/pii/S0019103513005393.

L. Ojha, M. B. Wilhelm, S. L. Murchie, A. S. McEwen, J. J. Wray, J. Hanley, M. Massé, and M. Chojnacki. Spectral evidence for hydrated salts in recurring slope lineae on Mars. *Nature Geoscience*, 8(11):829–832, Nov 2015. doi: 10.1038/ngeo2546.

A. Pommerol, N. Thomas, B. Jost, P. Beck, C. Okubo, and A. S. McEwen. Photometric properties of mars soils analogs. *Journal of Geophysical Research: Planets*, 118(10):2045–2072, 2013. doi: 10.1002/jgre.20158. URL https://agupubs.onlinelibrary.wiley.com/doi/abs/10.1002/jgre.20158.

N. E. Putzig, E. M. Barratt, M. T. Mellon, and T. I. Michaels. MARSTHERM: A Web-based System Providing Thermophysical Analysis Tools for Mars Research. In *AGU Fall Meeting Abstracts*, volume 2013, pages P43C–2023, Dec 2013.

R Core Team. *R: A Language and Environment for Statistical Computing*. R Foundation for Statistical Computing, Vienna, Austria, 2019. URL https://www.R-project.org/.

E. I. Schaefer, A. S. McEwen, and S. S. Sutton. A case study of recurring slope lineae (RSL) at Tivat crater: Implications for RSL origins. *Icarus*, 317:621–648, Jan 2019. doi: 10.1016/j.icarus.2018.07.014.

F. Schmidt, F. Andrieu, F. Costard, M. Kocifaj, and A. G. Meresescu. Formation of recurring slope lineae on Mars by rarefied gas-triggered granular flows. *Nature Geoscience*, 10(4):270–273, Mar 2017. doi: 10.1038/ngeo2917.

N. Schorghofer, J. Levy, and T. Goudge. High-resolution thermal environment of recurring slope lineae in palikir crater, mars, and its implications for volatiles. *Journal of Geophysical Research: Planets*, 0(ja), 2019. doi: 10.1029/2019JE006083. URL `https://agupubs.onlinelibrary.wiley.com/doi/abs/10.1029/2019JE006083`.

S. S. Shapiro and M. B. Wilk. An analysis of variance test for normality (complete samples). *Biometrika*, 52(3/4):591–611, 1965. ISSN 00063444. URL `http://www.jstor.org/stable/2333709`.

D. Shoji, S. Imamura, M. Nakamura, and R. Noguchi. Angle of repose of Martian wet sand using discrete element method: Implication for the seasonal cycle of recurring slope lineae(RSL) by relative humidity. *arXiv e-prints*, art. arXiv:1909.06144, Sep 2019.

E. Simioni, C. Re, T. Mudric, A. Pommerol, N. Thomas, and G. Cremonese. a Photogrammetric Pipeline for the 3d Reconstruction of Cassis Images on Board Exomars Tgo. *ISPRS - International Archives of the Photogrammetry, Remote Sensing and Spatial Information Sciences*, 62W1:133–139, Jul 2017. doi: 10.5194/isprs-archives-XLII-3-W1-133-2017.

L. J. Steele, M. R. Balme, S. R. Lewis, and A. Spiga. The water cycle and regolith–atmosphere interaction at gale crater, mars. *Icarus*, 289:56 – 79, 2017.

ISSN 0019-1035. doi: https://doi.org/10.1016/j.icarus.2017.02.010. URL http://www.sciencedirect.com/science/article/pii/S0019103516304845.

D. E. Stillman and R. E. Grimm. Two pulses of seasonal activity in martian southern mid-latitude recurring slope lineae (RSL). *Icarus*, 302:126–133, Mar 2018. doi: 10.1016/j.icarus.2017.10.026.

D. E. Stillman, T. I. Michaels, R. E. Grimm, and K. P. Harrison. New observations of martian southern mid-latitude recurring slope lineae (RSL) imply formation by freshwater subsurface flows. *Icarus*, 233:328–341, May 2014. doi: 10.1016/j.icarus.2014.01.017.

D. E. Stillman, T. I. Michaels, R. E. Grimm, and J. Hanley. Observations and modeling of northern mid-latitude recurring slope lineae (RSL) suggest recharge by a present-day martian briny aquifer. *Icarus*, 265:125–138, Feb 2016. doi: 10.1016/j.icarus.2015.10.007.

D. E. Stillman, B. D. Bue, K. L. Wagstaff, K. M. Primm, T. I. Michaels, and R. E. Grimm. Evaluation of wet and dry recurring slope lineae (rsl) formation mechanisms based on quantitative mapping of rsl in garni crater, valles marineris, mars. *Icarus*, 335:113420, 2020. ISSN 0019-1035. doi: https://doi.org/10.1016/j.icarus.2019.113420. URL http://www.sciencedirect.com/science/article/pii/S0019103519303835.

M. Tebolt, J. Levy, T. Goudge, and N. Schorghofer. Slope, elevation, and thermal inertia trends of martian recurring slope lineae initiation and termination points:

Multiple possible processes occurring on coarse, sandy slopes. *Icarus*, 338:113536, 2020. ISSN 0019-1035. doi: https://doi.org/10.1016/j.icarus.2019.113536. URL http://www.sciencedirect.com/science/article/pii/S0019103519305779.

N. Thomas, G. Cremonese, R. Ziethe, M. Gerber, M. Brändli, G. Bruno, M. Erismann, L. Gambicorti, T. Gerber, K. Ghose, M. Gruber, P. Gubler, H. Mischler, J. Jost, D. Piazza, A. Pommerol, M. Rieder, V. Roloff, A. Servonet, W. Trottmann, T. Uthaicharoenpong, C. Zimmermann, D. Vernani, M. Johnson, E. Pelò, T. Weigel, J. Viertl, N. De Roux, P. Lochmatter, G. Sutter, A. Casciello, T. Hausner, I. Ficai Veltroni, V. Da Deppo, P. Orleanski, W. Nowosielski, T. Zawistowski, S. Szalai, B. Sodor, S. Tulyakov, G. Troznai, M. Banaskiewicz, J. C. Bridges, S. Byrne, S. Debei, M. R. El-Maarry, E. Hauber, C. J. Hansen, A. Ivanov, L. Keszthelyi, R. Kirk, R. Kuzmin, N. Mangold, L. Marinangeli, W. J. Markiewicz, M. Massironi, A. S. McEwen, C. Okubo, L. L. Tornabene, P. Wajer, and J. J. Wray. The Colour and Stereo Surface Imaging System (CaSSIS) for the ExoMars Trace Gas Orbiter. *Space Sci. Rev.*, 212(3-4):1897–1944, Nov 2017. doi: 10.1007/s11214-017-0421-1.

J. Toner and D. Catling. Chlorate brines on mars: Implications for the occurrence of liquid water and deliquescence. *Earth and Planetary Science Letters*, 497:161 – 168, 2018. ISSN 0012-821X. doi: https://doi.org/10.1016/j.epsl.2018.06.011. URL http://www.sciencedirect.com/science/article/pii/S0012821X18303509.

M. Vincendon, Y. Langevin, F. Poulet, J.-P. Bibring, and B. Gondet. Recovery of surface reflectance spectra and evaluation of the optical depth of aerosols in the near-ir using a monte carlo approach: Application to the omega observations of high-latitude regions of mars. *Journal of Geophysical Research: Planets*, 112(E8), 2007. doi: 10.1029/2006JE002845. URL `https://agupubs.onlinelibrary.wiley.com/doi/abs/10.1029/2006JE002845`.

M. Vincendon, F. Forget, and J. Mustard. Water ice at low to midlatitudes on mars. *Journal of Geophysical Research: Planets*, 115(E10), 2010. doi: 10.1029/2010JE003584. URL `https://agupubs.onlinelibrary.wiley.com/doi/abs/10.1029/2010JE003584`.

M. Vincendon, C. Pilorget, J. Carter, and A. Stcherbinine. Observational evidence for a dry dust-wind origin of mars seasonal dark flows. *Icarus*, 325:115 – 127, 2019. ISSN 0019-1035. doi: https://doi.org/10.1016/j.icarus.2019.02.024. URL `http://www.sciencedirect.com/science/article/pii/S0019103518305712`.

A. Wang, Z. Ling, Y. Yan, A. S. McEwen, M. T. Mellon, M. D. Smith, B. L. Jolliff, and J. Head. Subsurface Cl-bearing salts as potential contributors to recurring slope lineae (RSL) on Mars. *Icarus*, 333:464–480, Nov 2019. doi: 10.1016/j.icarus.2019.06.024.

F. Wilcoxon. Individual comparisons by ranking methods. *Biometrics Bulletin*, 1 (6):80–83, 1945. ISSN 00994987. URL `http://www.jstor.org/stable/3001968`.